ROUGHNESS AND ANGULARITY OF STRENGTH-TESTED METEORITE FRAGMENTS. Gabriel Gowman[1], Erik Asphaug[1], Andrew Ryan[1], Desireé Cotto-Figueroa[2], and Laurence A.J. Garvie[3,4], [1]Lunar and Planetary Laboratory, University of Arizona, Tucson, AZ 85721 (gowmang@arizona.edu), [2]Dept. of Physics and Electronics, University of Puerto Rico Humacao, Humacao, PR 00792, [3]Buseck Center for Meteorite Studies, [4]School of Earth and Space Exploration, Arizona State University, Tempe, AZ 85287.

Introduction: Meteorites are fragments from asteroids and nearby planets; as such they contain unique information about solar system physical and chemical properties, as well as planetary origins and geology. Particle roughness is known to play a significant role in controlling interparticle contact forces on a microscopic level as well as macroscopic effects such as stiffness and shear strength for granular materials [1]. As such, textural properties may be an indicator of meteorites' strength properties.

We quantify the roughness and angularity of fragments of two meteorite types, and discuss the connection between roughness (that can be obtained from remote sensing) and measured strength properties [2].

Samples and Methodology: Here we analyze four fragments from the CV3 meteorite Allende [3] and five from the H5 meteorite Tamdakht [4]. Two samples from each meteorite are fragmental remains of destructive stress-to-failure experiments [2]. The fragments have masses of 1.68-8.55 g and volumes ranging from 0.48 to 2.48 cm^3. We used a Polyga C506 structured-light scanner to produce 3D models of our samples. This scanner has a spatial resolution of ~20-25 μm and accuracy ≥12 μm. Each sample had 24-30 scans taken at multiple orientations, and the scans were combined into complete models using FlexScan3D software. The scanning process took approximately 30-60 minutes per sample. The 3D models were then analyzed using two metrics, *roughness* and *angularity*. Some of the samples have significant flat, smooth faces that are remnants of the original cut surfaces. Before calculating the metrics, these smooth faces were removed from the models.

Roughness: We apply the root mean square (RMS) slope roughness metric θ_{RMS} of [5] as previously applied to asteroid (101955) Bennu. Here, the scanned 3D model is compared to a decimated version of the same model, and the roughness is computed as the original model's RMS slope relative to the simplified version:

$$\theta_{RMS} = \sqrt{\frac{\sum_{i=1}^{N} \vartheta_i^2 a_i |\cos \vartheta_i|}{\sum_{i=1}^{N} a_i |\cos \vartheta_i|}}$$

where a_i is the area of a particular facet and ϑ_i is the angle of that facet relative to the local horizontal, as defined by the coarsened model, in which we cut each scanned model down to 5% of its original facet count. In addition, we compute local roughness, $\theta_{RMS,i}$, by summing the metric restricted to each facet within the coarsened models.

Angularity: We calculate the 3D gradient-based angularity index AI_g defined by [6]. According to this method, we construct a degree 25 spherical harmonic model of each sample and re-evaluate this spherical harmonic model using an icosahedral grid of points that yields 81,920 facets. The 25th spherical harmonic degree is chosen by [6] as the division between angularity and finer texture. From there, the angularity index is:

$$AI_g = \frac{\sum_{i=1}^{N} \sum_{j=1}^{3} \theta_{ij}}{\sum_{i=1}^{N} \sum_{j=1}^{3} \theta'_{ij}} - 1$$

where θ_{ij} is the angle between two neighboring facets of the degree 25 model and θ'_{ij} is the corresponding angle for an ellipsoidal (degree 1) model of the sample. Thus spheres and ellipsoids have zero angularity, and relatively equidimensional samples have lower AI_g than more flattened or jagged samples.

Results: Global θ_{RMS} ranges from 8.21° to 9.15° for all samples from both meteorites. The range of AI_g is much wider, varying from 3.39 to 12.02. The local roughness $\theta_{RMS,i}$ for Allende Fragment 1, which has a global θ_{RMS} of 8.90°, is plotted in Fig. 2. Values of $\theta_{RMS,i}$ cover a similar range for all samples and fit log-normal curves well. The high-value areas broadly align with fracture scarps near edges, while the arcuate indentation on the lower-right is smooth.

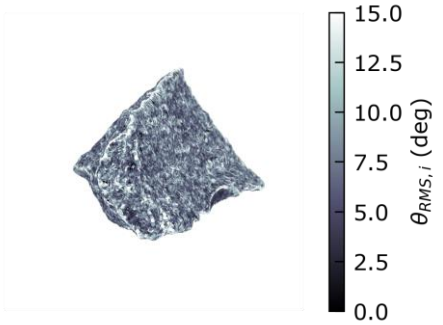

Figure 2: Local roughness for Allende Fragment 1. This sample is ~2 cm across.

The local angularity is defined as $AI_{g,i} = \sum_{j=1}^{3} \theta_{ij}$ such that

$$AI_g = \frac{\sum_{i=1}^{N} AI_{g,i}}{\sum_{i=1}^{N} AI'_{g,i}} - 1$$

with $AI'_{g,i}$ again calculated based on a degree 1 model. Fig. 3 plots $AI_{g,i}$ for the same sample, measured in

degrees. Color (and the values of $AI_{g,i}$ in the color bar) for this figure is on a $\log_{10}$ scale, restricted to the range from $10^{-0.75}$ to $10^{1.75}$ degrees.

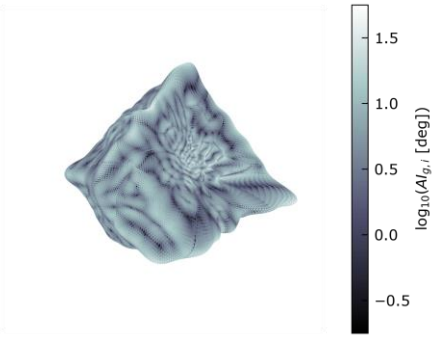

Figure 3: Local angularity for Allende Fragment 1.

As with the θ_{RMS} values, there is no clear separation between the Allende and Tamdakht samples. Indeed, the AI_g values for two samples with relatively cuboid shapes from each meteorite are similar, not just for the chosen model parameters, but at almost all model degrees and resolutions tested.

Even at the chosen target, degree 25, the spherical harmonic models (Fig. 3) fail to capture the sharp edges of the samples. This is especially clear for the highly jagged samples in our study. Higher-degree models capture more of the angularity, but it would take an extremely high-degree spherical harmonic model to fully capture the samples' angularity and separate similarly shaped samples. Additionally, the spatial distribution of angularity (Fig. 3) shows ring-like "ridges" that are artifacts of the spherical harmonic model rather than actual features of the sample. The data suggest that the angularity metric AI_g as defined and applied by [6] is insufficient to describe these highly angular samples, and is better suited to relatively round or equidimensional particles.

Angularity-roughness correlation: We plot the whole-sample values of θ_{RMS} vs. AI_g in Fig. 4 with linear regression on the sample data, both together and by meteorite. Although they quantify different properties, they appear to be negatively correlated, for Allende samples in particular.

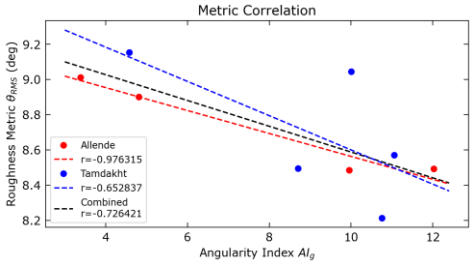

Figure 4: θ_{RMS} vs. AI_g for all nine samples.

Relationship to strength: The Tamdakht samples depart significantly from a linear fit, while the Allende samples follow an apparent trend (Fig. 4). This may be related to Tamdakht being significantly more heterogeneous in compressive strength than Allende [2]; this is currently being explored.

Conclusions and Future Work: For now, we are unable to separate a collection of samples from Allende and Tamdakht based on values of θ_{RMS} and AI_g alone with the chosen parameters. Furthermore, the correlations between the two metrics (Fig. 4) have similar slopes, suggesting that a collection of samples from Allende and Tamdakht would not be readily separable based on a combined analysis either. The roughness metric, however, accurately describes sample roughness on a local level and will be useful in further analysis of meteorite breakage.

In future work, we shall fold in the strength measurements from [2] and ongoing work creating fragments from stress-to-failure tests. This is a first step toward connecting remote sensing quantities, such as fracture roughness to strength properties of asteroidal materials, and has significant implications for planetary defense.

Acknowledgments: This material is based on work supported by the National Aeronautics and Space Administration under Grant No. 80NSSC21K1983 issued through the Yearly Opportunities for Research in Planetary Defense (YORPD) Program. We gratefully acknowledge use of OSIRIS-REx lab space and materials for the scanning of our samples, and the Buseck Center for Meteorite Studies for the meteorites. The OSIRIS-REx lab space and materials were funded in part by NASA Contract NNM10AA11C issued through the New Frontiers Program.

References: [1] Su, D. et al. (2019) *Powder Technol., 356,* 423-438. [2] Cotto-Figueroa, D. et al. (2016) *Icarus, 277,* 73-77. [3] King, E. A. et al. (1969) *Science, 163,* 928-929. [4] Weisberg, M. K. et al. (2009) *Meteorit. Planet. Sci., 44,* 429-462. [5] Rozitis, B. et al. (2020) *Sci. Adv.,* 6(41):eabc3699. [6] Su, D. et al. (2020) *Powder Technol., 364,* 1009-1024.